Supplement of Hydrol. Earth Syst. Sci., 30, 7177–7195, 2026
https://doi.org/10.5194/hess-30-7177-2026-supplement
© Author(s) 2026. CC BY 4.0 License.



Hydrology and Earth System Sciences
Open Access
EGU

Supplement of

Characterizing runoff response to rainfall in permafrost catchments and its implications for hydrological and biogeochemical fluxes in a warming climate

Cansu Culha et al.

Correspondence to: Cansu Culha (cansu.culha@gmail.com) and James W. Kirchner (kirchner@env.eth.ch)

The copyright of individual parts of the supplement might differ from the article licence.

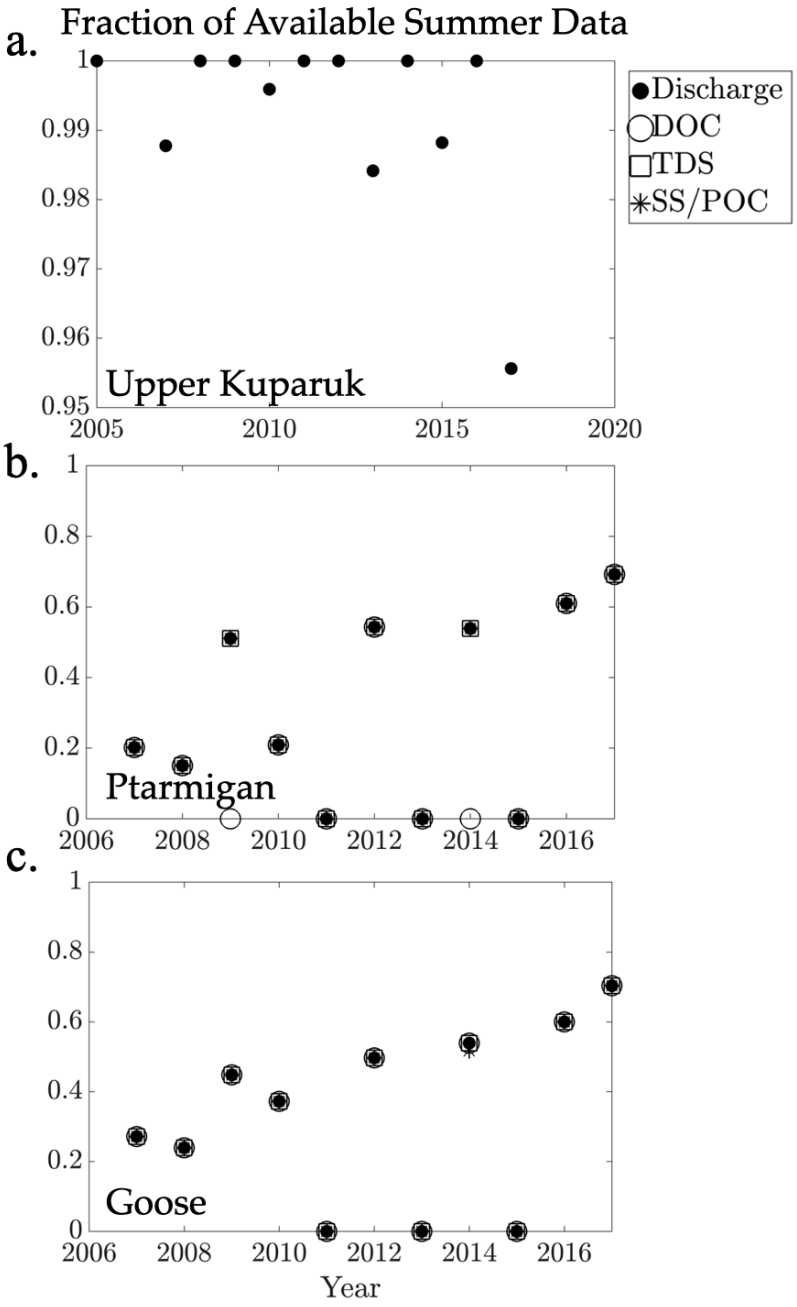


Figure S1. Fraction of available data during the summer months for the Upper Kuparuk (a), Goose (b), and Ptarmigan (c) catchments. Solid markers indicate discharge data availability, while open circle markers represent material-flux data availability. Among the three sites, Upper Kuparuk (a) has the most consistent coverage, with over 95% discharge data availability in most years. In contrast, both Goose (b) and Ptarmigan (c) catchments at Cape Bounty include material flux data but have less consistent overall coverage.

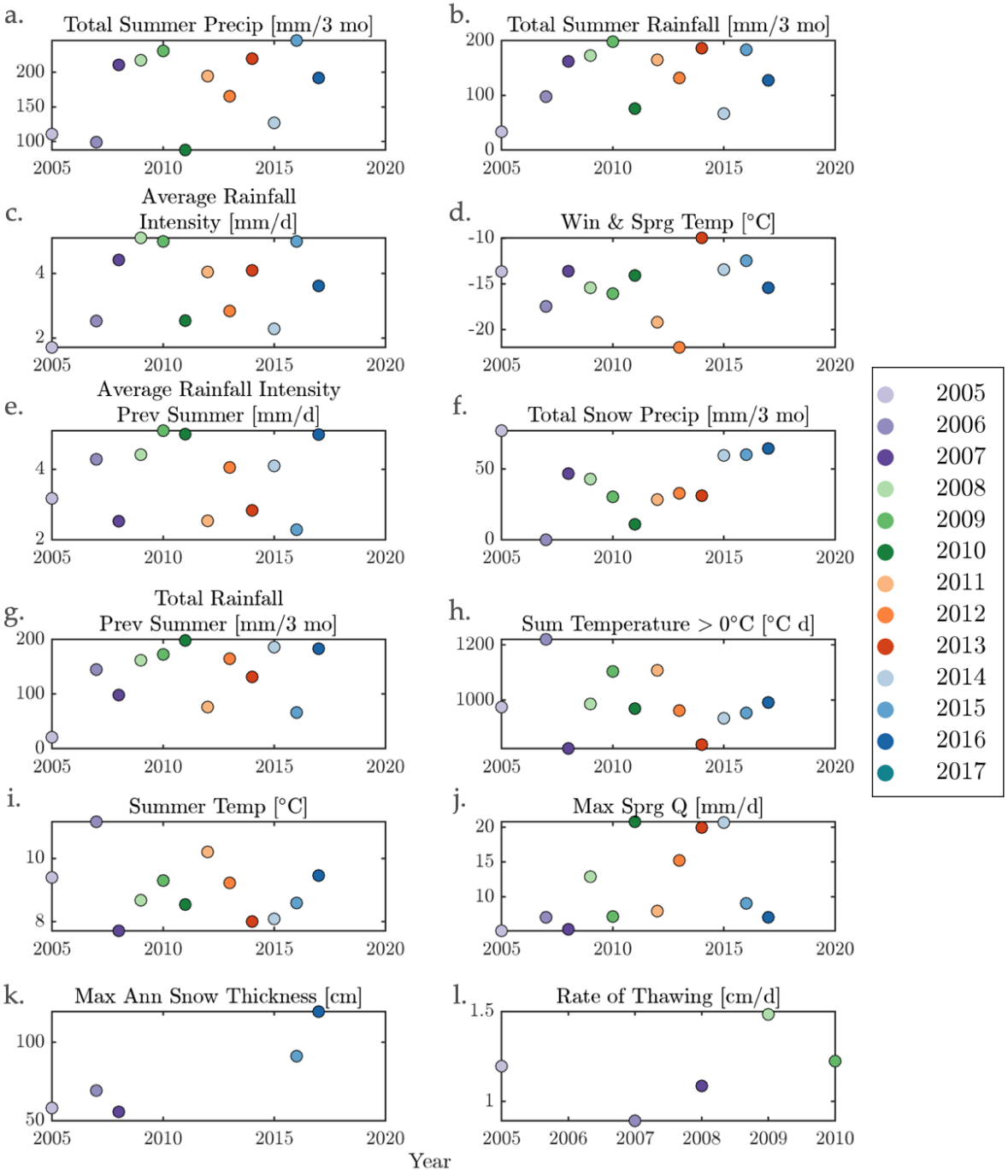


Figure S2. Time series of potential explanatory variables for runoff response at Upper Kuparuk. Each color represents a distinct year and is used consistently throughout the manuscript. To improve visual grouping, we use light to dark shading within a color family to represent three consecutive years before switching to a new base color. We evaluate 12 potential explanatory variables: (a) total summer precipitation, (b) total summer rainfall, (c) average rainfall intensity, (d) average temperatures during the preceding winter and spring, (e) average rainfall intensity of the previous summer, (f) total snowfall, (g) total summer precipitation of the previous summer, (h) cumulative number of degree days above 0 °C, (i)

average summer temperature, (j) maximum spring streamflow, (k) maximum snow depth, and (l) rate of thawing. The plot titles correspond to the y-axis. Full descriptions of how each variable was derived are provided in the Methods section. Note that maximum snow depth and rate of thawing are only available for five years and are included as context.

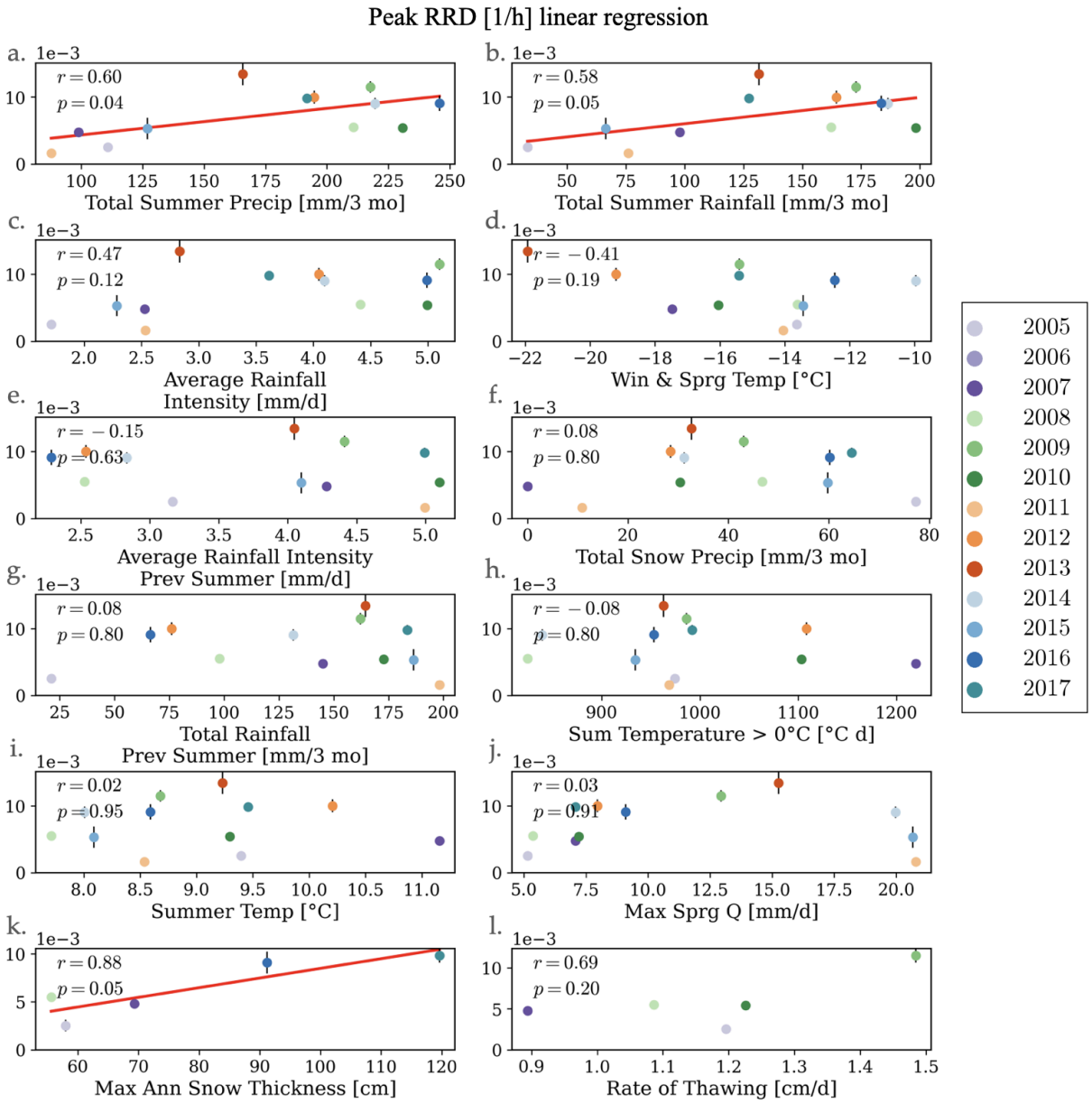


Figure S3. Linear regression between each explanatory variable in Supp. Fig. 2 and runoff response distribution (RRD) peak height at Upper Kuparuk. The potential explanatory variables are shown along the x-axis: (a) total summer precipitation, (b) total summer rainfall, (c) average rainfall intensity, (d) average temperatures during the preceding winter and spring, (e) average rainfall intensity of the previous summer, (f) total snowfall, (g) total summer precipitation of the previous summer, (h) cumulative number of degree days above 0 $^{\circ}$C, (i) average summer temperature, (j) maximum spring streamflow, (k) maximum snow depth, and (l) rate of thawing. Note that maximum snow depth and rate of thawing are only available for five years and are included as context.

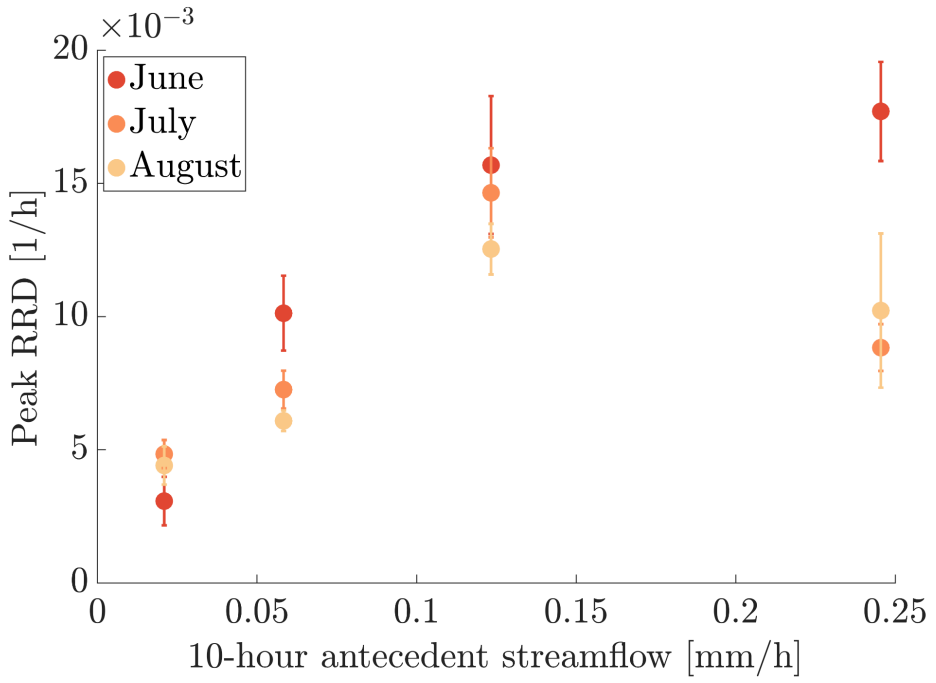


Figure S4. Peak runoff response as a function of antecedent streamflow, showing that runoff is more sensitive to antecedent streamflow than to the month in which it occurs. We bin peak runoff responses by antecedent streamflow and compare the results across June, July, and August. The antecedent streamflow binning is the same as in **Man. Fig. 2**. In all months, peak runoff response increases with antecedent streamflow, except in the highest bin, which is based on fewer events: 44 for June, 38 for July, and only 11 for August. By contrast, the other bins each contain an average of 50 events. Across all bins, the months exhibit similar peak runoff responses, with the lowest responses occurring at the lowest antecedent streamflow. June displays the highest peak runoff response at high antecedent streamflow levels.

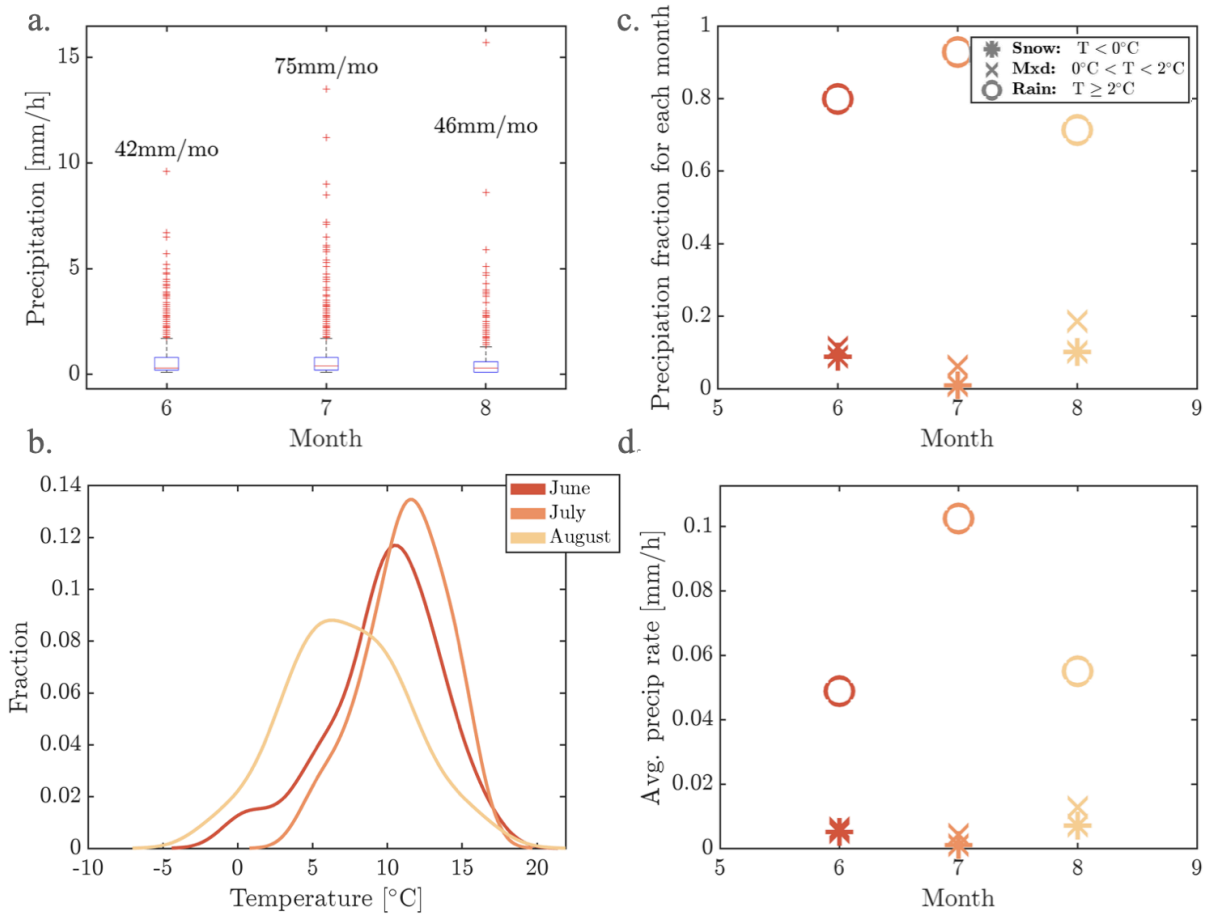


Figure S5. Rainfall and temperature patterns across summer months (June is red, July is orange, and August is yellow). (a) The average precipitation for each hour with nonzero precipitation; cumulative monthly precipitation is shown above each boxplot. (b) Hourly temperature distribution for each month. (c) Average hourly precipitation by precipitation type, classified by temperature during precipitation. (d) Average precipitation rate per hour with rain. Note that higher precipitation rates in July (panel d) do not necessarily yield proportionally higher monthly totals (panel a), as total precipitation also depends on the duration of rainfall events. Circle, cross, and star correspond to rain, mixed precipitation, and snow, respectively, in (b) and (d).

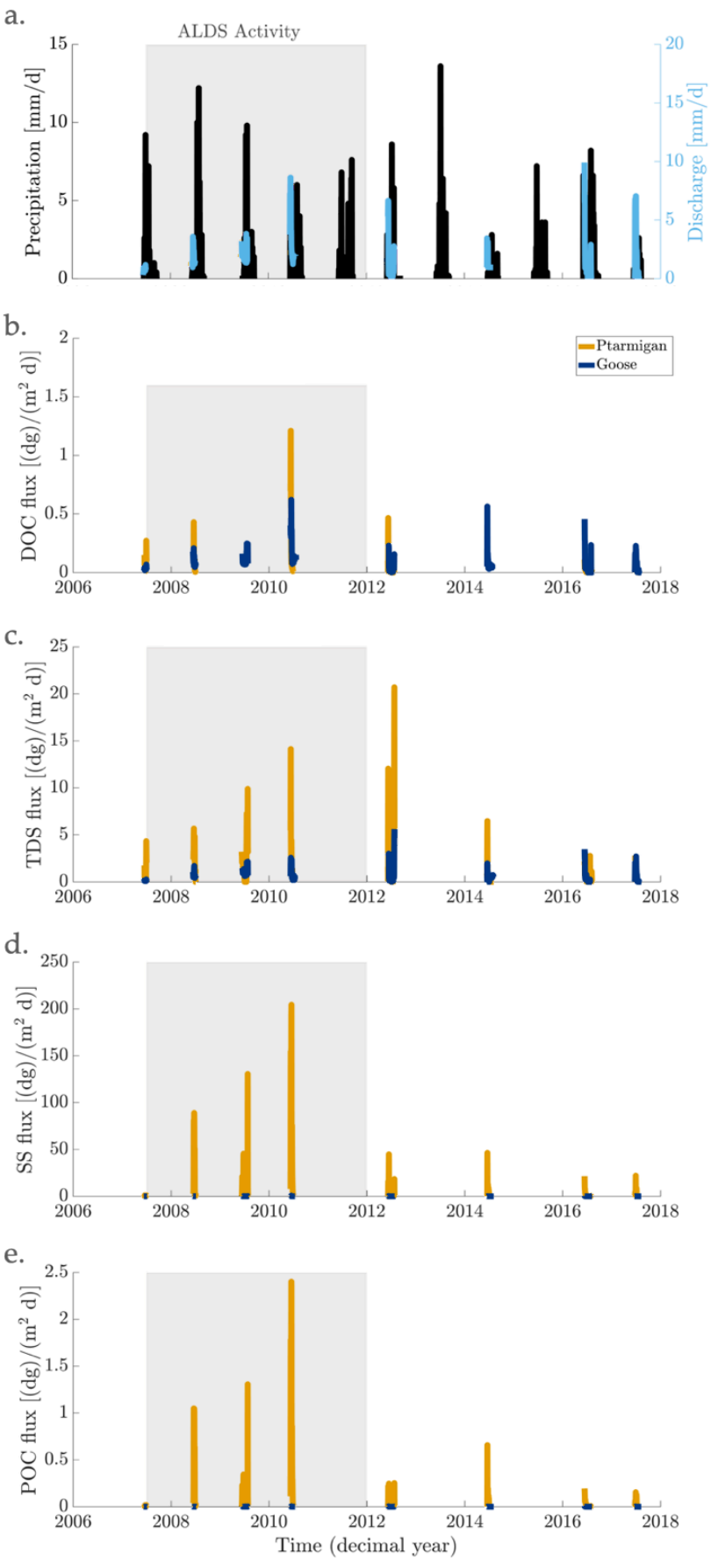


Figure S6. Time-series comparison of daily precipitation, discharge, and material fluxes at the Ptarmigan catchment (with active layer detachments (ALDs), orange) and the Goose catchment (without ALDs, dark blue). The light-gray shading (late-2007 to 2011) delineates the interval when active layer detachments (ALDs) are actively eroding at Ptarmigan. Panel (a) shows daily totals of summer precipitation (black) and discharge (light blue). Panels (b)–(e) present dissolved organic carbon (DOC), total dissolved solids (TDS), suspended sediment (SS), and particulate organic carbon (POC) fluxes, respectively; fluxes are calculated as concentration multiplied by discharge and are expressed as milligrams of material per area per day (mg m^{-2} d^{-1}). During the ALD interval, DOC flux is elevated at Ptarmigan but subsequently declines such that Goose becomes the larger DOC source. TDS flux is persistently higher at Ptarmigan and rises further while the slides are active. SS and POC fluxes at Ptarmigan increase by an order of magnitude during ALD activity, whereas both fluxes remain minimal at Goose throughout the record.

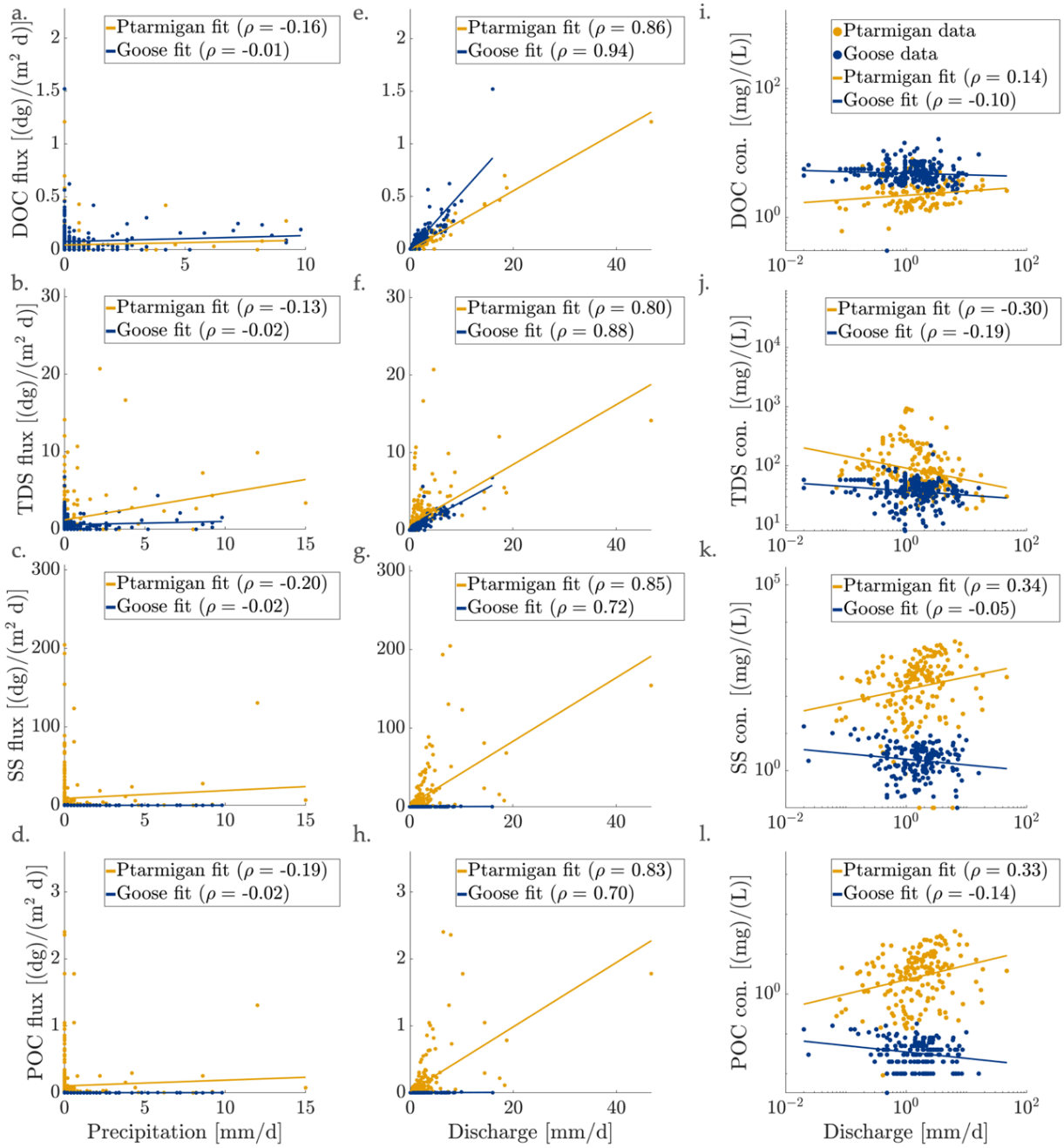


Figure S7. Correlation between precipitation [(a)–(d)] and discharge [(e)–(h)] with material fluxes [(a)-(h)] and concentrations [(i)-(l)] in the Ptarmigan catchment (with active layer detachments [ALDs], orange) and the Goose catchment (without ALDs, blue). Panels show dissolved organic carbon (DOC), total dissolved solids (TDS), suspended sediment (SS), and particulate organic carbon (POC) fluxes and concentrations. Panels [(i) - (l)] are on a log-log scale. There is no clear correlation between precipitation and material fluxes, nor between discharge and material concentrations at either catchment. In contrast, discharge shows a positive correlation with material flux, particularly for TDS, SS, and POC at Ptarmigan. Goose shows higher DOC flux with increasing discharge, while Ptarmigan exhibits greater TDS, SS, and POC fluxes.